DEMENTIAS - ORIGINAL ARTICLE

New diagnostic EEG markers of the Alzheimer's disease using visibility graph

Mehran Ahmadlou · Hojjat Adeli · Anahita Adeli

Abstract A new chaos–wavelet approach is presented for electroencephalogram (EEG)-based diagnosis of Alzheimer's disease (AD) employing a recently developed concept in graph theory, visibility graph (VG). The approach is based on the research ideology that nonlinear features may not reveal differences between AD and control group in the band-limited EEG, but may represent noticeable differences in certain sub-bands. Hence, complexity of EEGs is computed using the VGs of EEGs and EEG sub-bands produced by wavelet decomposition. Two methods are employed for computation of complexity of the VGs: one based on the power of scale-freeness of a graph structure and the other based on the maximum eigenvalue of the adjacency matrix of a graph. Analysis of variation is used for feature selection. Two classifiers are applied to the selected features to distinguish AD and control EEGs: a Radial Basis Function Neural Network (RBFNN) and a two-stage classifier consisting of Principal Component Analysis (PCA) and the RBFNN. After comprehensive statistical studies, effective classification features and mathematical markers were discovered. Finally, using the discovered features and a two-stage classifier (PCA-RBFNN), a high diagnostic accuracy of 97.7% was obtained.

Keywords Alzheimer's disease · EEG · Visibility graph

Introduction

Alzheimer's disease (AD) is the most common dementia defined as an organic neurodegenerative and progressive dementia characterized by deficient episodic memory and cognitive functions such as sensory gating, remembering,

M. Ahmadlou
Department of Biomedical Engineering,
Amirkabir University of Technology, Tehran, Iran

H. Adeli (✉)
Department of Biomedical Engineering,
The Ohio State University, 470 Hitchcock Hall,
2070 Neil Avenue, Columbus, OH 4310, USA
e-mail: adeli.1@osu.edu

H. Adeli
Department of Biomedical Informatics,
The Ohio State University, 470 Hitchcock Hall,
2070 Neil Avenue, Columbus, OH 4310, USA

H. Adeli
Department of Civil and Environmental Engineering
and Geodetic Science, The Ohio State University,
470 Hitchcock Hall, 2070 Neil Avenue,
Columbus, OH 4310, USA

H. Adeli
Department of Electrical and Computer Engineering,
The Ohio State University, 470 Hitchcock Hall,
2070 Neil Avenue, Columbus, OH 4310, USA

H. Adeli
Department of Neurological Surgery, The Ohio State University,
470 Hitchcock Hall, 2070 Neil Avenue, Columbus,
OH 4310, USA

H. Adeli
Department of Neuroscience, The Ohio State University,
470 Hitchcock Hall, 2070 Neil Avenue, Columbus,
OH 4310, USA

A. Adeli
Department of Neurology, University of Pittsburgh,
Pittsburgh, PA 15213, USA

reasoning, and planning (Dierks et al. 1997; Jeong et al. 2001; Hiele et al. 2007; Bouwman et al. 2009; Thomas et al. 2010). It is one of the most prevalent diseases in elderly afflicting about 5 million individuals in the US alone and more than 26.6 million individuals worldwide (Jackson and Snyder 2008). Loss of neuronal synapses (Hampel et al. 2002; Adeli et al. 2005a), axonal degeneration, and neuronal cell body death (Fjell et al. 2010) in AD result in changes in various regions of the brain anatomically (structurally) and physiologically (functionally) (Head et al. 2005). Although autopsy is the only possible way for a definite diagnosis of AD, researchers have been trying to diagnose AD based on studies of computer imaging technologies (Thompson et al. 1998, 2001; Jones et al. 2006; Stebbins and Murphy 2009), electroencephalograms (EEGs), and magneto-encephalograms (MEGs) (Adeli et al. 2005a). Since the microscopic changes and brain dynamics cannot be detected by computer imaging techniques (which have low temporal resolution), diagnosis of AD in its early stages through EEG and MEG appears to be more promising (Dierks et al. 1997; Lee et al. 2007; Osterhage et al. 2007; Kramer et al. 2007). Although many studies have been performed on frequency changes in EEG and MEG signals, such as the well-known EEG slowing (Giannitrapani et al. 1991; Adler et al. 2003), increased power of EEG in gamma band (40–70 Hz) (Deursen et al. 2008), and increased 40-Hz steady-state response measured through MEG (Osipova et al. 2006) and EEG (Deursen et al. 2009), these studies cannot describe the highly complex dynamics of the brain of AD patients where complexity features are influenced greatly by loss of synapses and functional and structural changes.

Adeli et al. (2005a) presented a state-of-the-art review of research performed on computational modeling of AD and its markers based on the following approaches: computer imaging, classification models, connectionist neural models, and biophysical neural models. They concluded that a mixture of markers and a combination of novel computational techniques such as neural computing, chaos theory, and wavelets can increase the accuracy of algorithms for automated detection and diagnosis of AD. In a complementary article, Adeli et al. (2005b) presented a state-of-the-art review of models of computation and analysis of EEGs for diagnosis and detection of AD using time–frequency analysis, wavelet analysis, and chaos analysis.

Chaos theory provides two types of complexity measures: correlation dimension (CD) as a measure of complexity of a trajectory in its embedding space, and fractal dimension (FD) as a measure of self-similarity and complexity of a time series computed directly without reconstruction of the embedding space (Gomez et al. 2009; Rossello et al. 2009; He et al. 2010). Besthorn et al. (1995) report lower CD in AD EEGs than control EEGs in the entire band-limited EEG (0.5–30 Hz) in eyes closed resting state. Besthorn et al. (1997) report accuracy of 69.5%, in distinguishing AD from healthy subjects, based on the CD. Also, applying Principal Component Analysis (PCA) (Wu and Ben-Arie 2008; Lopez-Rubio and Ortiz-de-Lazcano-Lobato 2009) to a feature space consisting of CD, various frequency features (related to power of EEG sub-bands), and coherence, and adding the age of subjects as an auxiliary feature, they report an accuracy of 90%. Jelles et al. (1999) found lower CD in AD EEGs compared with healthy EEGs in three conditions: eyes closed, eyes open, and during an arithmetic task (p value = 0.023). Jeong et al. (2001) report reduced CD in the entire EEG of AD brain compared with healthy EEGs in most regions.

Using Hausdorf's FD, Woyshville and Calabrese (1994) detected decreased complexity in occipital loci of AD patients based on studies of EEGs in resting eyes closed condition. Recently, Gomez et al. (2009) reported reduced Higuchi's FD (HFD) (Higuchi 1988), in MEG of AD patients compared with healthy individuals with a detection accuracy of 87.8%. MEG, however, is very sensitive to environmental noise and hence needs an isolation room and very specific amplifiers. Although EEG has some limitations such as effects of neighboring electrodes, it is a more accessible diagnostic device and with automated signal processing techniques can be powerful in diagnostic applications.

Recently, Adeli et al. (2008) presented a multi-paradigm spatio-temporal wavelet–chaos methodology for analysis of EEGs and their sub-bands for discovering potential markers of abnormality in AD. The nonlinear dynamics of the EEG and EEG sub-bands are quantified in the form of CD, representing system complexity, and the largest Lyapunov exponent (LLE), representing system chaoticity. They found that the wavelet–chaos methodology and the sub-band analysis developed in their research accurately characterize the nonlinear dynamics of any non-stationary EEG-like signals. They also concluded that changes in the brain dynamics are not spread out equally across the spectrum of the EEG and over the entire brain, but are localized in certain frequency bands and electrode loci.
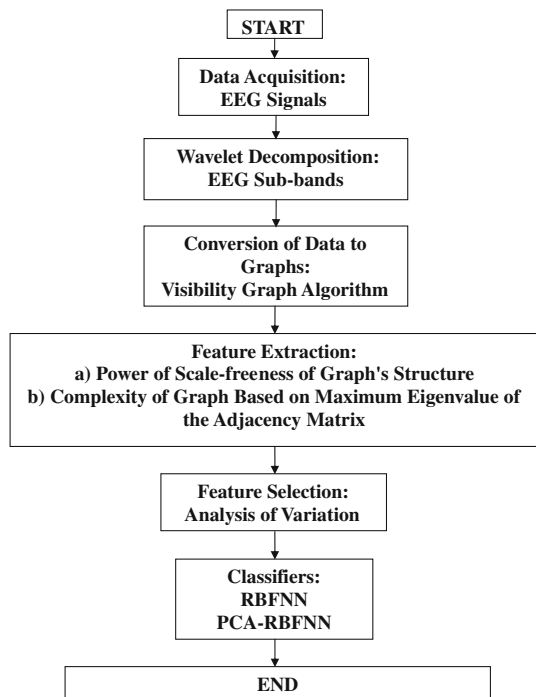
Recently, a new and simple method was introduced to convert a time series to a graph, called visibility graph (VG), and its structure was shown to be related to fractality (self-similarity) and complexity of the time series (Lacasa et al. 2008). Since quantification of complexity and self-similarity of a graph does not need many nodes in the graph, computation of complexity of a time series does not need many time samples when it is converted to a graph.

The authors investigate whether VG can be used as an effective tool for diagnosing AD. In this article, a new chaos–wavelet approach is presented for EEG-based diagnosis of AD employing VG. Following Adeli et al. (2007), the approach presented in this paper is based on the

research ideology that nonlinear features, such as CD or FD, may not reveal differences between AD and control group in the band-limited EEG, but may represent noticeable differences in certain sub-bands. Hence, following Adeli et al. (2007) and employing their wavelet–chaos methodology, in this study complexity of EEGs is computed using the VGs of EEGs and EEG sub-bands produced by wavelet decomposition. Two methods are employed for computation of complexity of the VGs: one based on the power of scale-freeness of a graph structure (Lacasa et al. 2008) and the other based on the maximum eigenvalue of the adjacency matrix of a graph (Kim and Wilhelm 2008). Analysis of variation (ANOVA) is used for feature selection. Then, two classifiers are applied to the selected features to distinguish AD and control EEGs: a Radial Basis Function Neural Network (RBFNN) and a two-stage classifier consisting of PCA and the RBFNN.

Method

Figure 1 shows a flowchart for the research approach presented in the paper which includes: wavelet decomposition of the band-limited EEGs into four sub-bands (Adeli et al. 2003), mapping the EEG sub-bands to their VGs and computing associated complexities two different ways, statistical analysis of the extracted complexities to discover the most discriminating/distinguishing features for AD diagnosis, and a classification between AD and control

```
           ┌──────────┐
           │  START   │
           └────┬─────┘
                │
    ┌───────────▼──────────┐
    │  Data Acquisition:   │
    │     EEG Signals      │
    └───────────┬──────────┘
                │
    ┌───────────▼──────────┐
    │ Wavelet Decomposition:│
    │    EEG Sub-bands     │
    └───────────┬──────────┘
                │
    ┌───────────▼──────────┐
    │ Conversion of Data to │
    │       Graphs:        │
    │ Visibility Graph Algorithm│
    └───────────┬──────────┘
                │
 ┌──────────────▼──────────────┐
 │     Feature Extraction:     │
 │ a) Power of Scale-freeness of Graph's Structure│
 │ b) Complexity of Graph Based on Maximum Eigenvalue of│
 │    the Adjacency Matrix     │
 └──────────────┬──────────────┘
                │
    ┌───────────▼──────────┐
    │  Feature Selection:  │
    │ Analysis of Variation│
    └───────────┬──────────┘
                │
    ┌───────────▼──────────┐
    │     Classifiers:     │
    │        RBFNN         │
    │      PCA-RBFNN       │
    └───────────┬──────────┘
                │
           ┌────▼─────┐
           │   END    │
           └──────────┘
```

Fig. 1 Flowchart for the research approach presented in the paper

groups based on the set of features selected across the various loci and sub-bands in the previous step.

Wavelet analysis

Following Adeli et al. (2007), using a three-level wavelet decomposition, the band-limited EEG (0–30 Hz) is decomposed into four sub-bands: beta (15–30 Hz) (β), alpha (8–15 Hz) (α), theta (4–8 Hz) (θ), and delta (0–4 Hz) (δ). Therefore, this step results in 95 {19 [7 (AD) + 12 (normal)] × 5 [4 (EEG sub-bands) + 1 (band-limited EEG)]} signals for each state (eyes open and eyes closed).

VG

Recently, Lacasa et al. (2008, 2009) presented VG and showed that such a graph inherits some of the properties of the time series such as periodic series resulting in regular graphs, random series resulting in random graphs, and fractal series converting into scale-free networks. Scale-free refers to the property that distribution of graph degrees (degree of a vertex is the number of edges connected to it) is determined by a power law independent of the number of nodes. For example, if the power is 2 it means one node has a power of 2, say 2^5, number of edges and two nodes exist each with 2^4 edges, four nodes each with 2^3 edges, 8 nodes each with 2^2 edges, and 16 nodes with 2^1 edges. The few nodes with very high degrees are called hubs. To the best of the authors' knowledge, this is the first application of the VG in EEG analysis.

VG of the time series $\mathbf{x}$ is constructed in the following manner: Consider the ith node of the graph, a_i, corresponds to the ith point of the time series, x_i. Two vertices (nodes) of the graph, a_m and a_n, are connected via a bidirectional edge if and only if:

$$x_{m+j} < x_n + \left(\frac{n-(m+j)}{n-m}\right)(x_m - x_n) \quad \forall j \in Z^+; j < n-m. \tag{1}$$

Figure 2 illustrates the procedure of converting time series $\mathbf{x}$ (Fig. 2a) to its VG (Fig. 2b). The gray line between x_i and x_j in Fig. 2a shows x_i and x_j can *see* each other. If and only if x_i and x_j can see each other, the corresponding vertexes of the VG, a_i and a_j, connect together through a bidirectional edge. Some dynamical features of the time series, such as complexity and self-similarity, hidden in the signal may be revealed in the structure of the resulting VG (Lacasa et al. 2008, 2009).

Complexity of VG

Complexity and fractality (self-similarity) of a time series can be obtained through estimation of complexity of its VG

Fig. 2 Illustration of
converting a time series $\{x_i\}$
shown in **a** to its visibility graph
with node sequence $\{a_i\}$ shown
in **b**. The *gray line* between x_i
and x_j in **a** shows x_i and x_j can
see each other. If and only if x_i
and x_j can see each other, the
corresponding vertexes of the
graph, a_i and a_j, connect
together through an edge. *Gray
lines* and *curves* show the edges
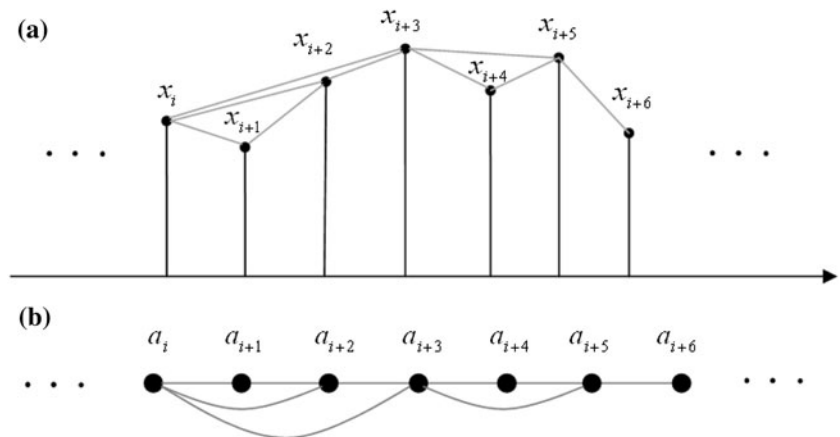
quickly similar to computation of FD without the need to
create the state space which requires a large number of
sampling points. Two methods are investigated for mea-
suring the complexity of VG in this research.

Power of scale-freeness in visibility graph (PSVG)

Using the VG algorithm, a periodic signal is mapped into
an ordered graph where all of its nodes connect to the same
number of edges and a fractal time series is mapped into a
graph with a scale-free structure which is characterized by:
$P(k) = k^{-r}$, where k indicates the order of a node, i.e. the
number of edges connected to a node, P is the probability
distribution of edges distributed in vertices or nodes of
a graph, and r is called the power of the scale-freeness.
Lacasa et al. (2008, 2009) show that the power of the scale-
free structure (r) of the VG indicates the amount of the
signal's fractality, and slope of $P(k)$ versus $1/k$ in a log–log
plane indicates the FD of the signal.

Adjacency matrix of an unweighted bidirectional graph
is a symmetric matrix indicating which nodes are con-
nected together. The elements of this matrix are 1 or 0
indicating the corresponding nodes are connected or not,
respectively. Figure 3a shows a sample healthy EEG with
1,024 sampling times. Figure 3b shows the degree
sequence of the corresponding VG which has 1,024 nodes
(the same as the number of sampling times). The ith ele-
ment of the sequence indicates the degree of the ith node of
VG. Figure 4 shows the 1,024 × 1,024 adjacency matrix
of the VG of the EEG shown in Fig. 3a where black dots
represent 1 or existence of an edge between the corre-
sponding nodes and whites represent zeros for no edge.
Since two sequential points of the time series can see each
other (according to the visibility definition of the VG
algorithm described earlier), all sequential nodes are con-
nected together. They make the diagonal of the adjacency
matrix. In the adjacency matrix of Fig. 4, black dots are
located mostly close to the diagonal of the matrix. But
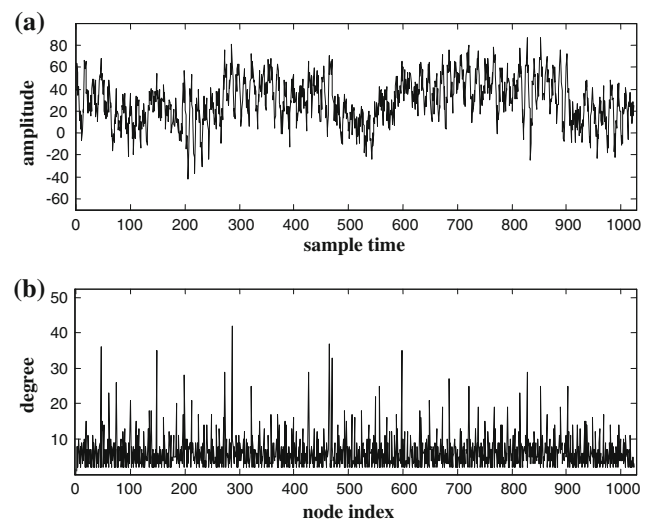
Fig. 3 **a** A sample healthy EEG and **b** degree sequence of its VG

there are also a few dots far away from the diagonal. Such
dots indicate that the corresponding node pair are far from
each other but are able to see each other. That is, such
nodes are hubs of the graph which correspond to points
with large or small values in the time series. Their large-
ness and smallness (compared with other points) makes
them visible by many other points which in turn causes
their correspond nodes to be the hubs of the VG.

In Fig. 5, values of $\log_2[P(k)]$ are plotted versus
$\log_2(1/k)$ [a small log base of 2 is used because we have a
relatively small sampling times (1,024) which makes it
more suitable than a log base of 10] and a least square fit is
used to obtain the value of the slope known as PSVG as a
measure of complexity and fractality of the EEG signal.

Graph index complexity (GIC)

As another measure of complexity of a graph, GIC (Kim
and Wilhelm 2008) is investigated in this research for
EEG-based diagnosis of AD. Let $\lambda_{\max}$ be the largest
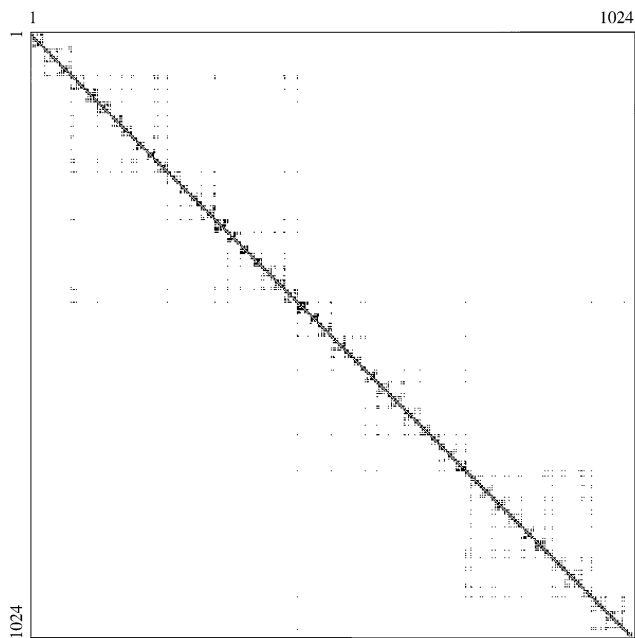
Fig. 4 Adjacency matrix of the VG of the EEG shown in Fig. 3a (*black dots* represent 1 and *whites* represent 0)
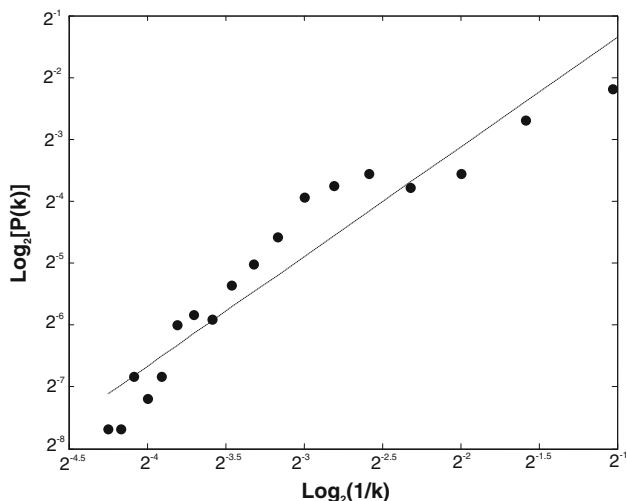
Fig. 5 Plot of $\log_2[P(k)]$ versus $\log_2(1/k)$ for the VG of the sample healthy EEG shown in Fig. 3, in a log–log plane. *Dashed line* is the fitted line to the *dots* through the least square (LS) method. The corresponding PSVG is slope = 1.75

eigenvalue of the adjacency matrix of a graph with n nodes. GIC is defined as follows:

$$C_{\lambda_{max}} = 4c(1-c) \tag{2}$$

where

$$c = \frac{\lambda_{max} - 2\cos(\pi/(n+1))}{n - 1 - 2\cos(\pi/(n+1))}. \tag{3}$$

It can be shown $C_{\lambda_{max}}$ varies between 0 and 1 because the following inequality is true for all unweighted bidirectional graphs (Kim and Wilhelm 2008):

$$2\cos(\pi/(n+1)) \le \lambda_{max} \le n - 1. \tag{4}$$

The more complex the graph's structure, the larger will be $C_{\lambda_{max}}$. In this research, application of this complexity measure to VG is called VGIC.

Statistical analysis and feature selection

In order to determine and evaluate the ability of features to discriminate groups based on variations both between and within groups based on PSVG or VGIC and reduce the input dimension for the final classification step, the one-way ANOVA is used.

One-way ANOVA produces a number called p value to evaluate the discriminating ability of the feature. It varies between 0 and 1 where a p value close to 0 indicates the high ability of the feature to discriminate the groups and a p value close to 1 indicates high similarity and closeness of distribution of the groups. Using this statistical tool, the most discriminating PSVGs and VGICs to distinguish the AD patients from control subjects are found in both eyes closed and eyes open conditions using a threshold p value of 0.001.

PCA

PCA is a statistical method of mapping data, linearly, into a space with a lower dimension. The mapping is usually done through a linear singular value decomposition (Lipovetsky 2009). The main goal of applying PCA to an input data set and using the outcome of the PCA analysis as input to a classifier is dimensional reduction of the input space without compromising the accuracy of the classification (Ghosh-Dastidar et al. 2008). Principal components are eigenvectors of the covariance matrix of the data with the highest eigenvalues, which show directions of maximum variations in the input data. The principal components are considered as axes of the new input space.

In this research, the input data of the PCA are the discriminative features obtained from the ANOVA. The number of appropriate eigenvectors for constructing the new feature space is obtained by trial and error so that the number of the features is sufficiently fewer than the number of data. A very rough guideline would be about 10% of the number of available data set.

Classification

In this step, the EEG data are classified into control and AD groups. The classifier used in this research is the RBFNN (Karim and Adeli 2003; Pedrycz et al. 2008; Anand et al. 2009; Savitha et al. 2009; Junfei and Honggui 2010; Ahmadlou and Adeli 2010; Wu et al. 2010) with PCA (PCA-RBFNN) and without PCA.

PCA-RBFNN consists of two stages: PCA and RBFNN. Inputs of the RBFNN are outputs of the PCA. RBFNN consists of an input node, one hidden radial basis function layer and an output layer. The number of nodes in the input layer is equal to number of the principal components produced by PCA. The number of nodes in the hidden layer is found based on the data used for training the network to yield the most accurate results as described in the next section. Neuron of the output layer has a hard limiter function which determines the group the data belongs to it. The outputs 1 and 0 correspond to AD group and control group, respectively. The weighted input to the radial basis transfer functions of the hidden layer is the Euclidian distance between the input vector and the weight matrix of links connecting the input neurons to the hidden layer's nodes, multiplied by a bias value. The bias changes the spread of the radial basis functions, which can be tuned for different distributions of data set in order to obtain the best classification results. A decrease in the distance between the weight vector and the input vector results in an increase in the output. The weights and biases are obtained by training the neural network to minimize the misclassification error in a mean square error (MSE) sense.

Data acquisition

The data set includes 19-channel EEGs (according to 10-20 standard system) from two different groups of subjects: 7 healthy elderly (control group; with average age of 71 (range 61–83) with no history of neurological or psychiatric disorder and 20 probable AD patients (average age of 74, range 53–85) diagnosed through National Institute of Neurological and Communicative Disorders and Stroke and the Alzheimer's Disease and Related Disorders Association (NINCDS-ADRDA) and Diagnostic and Statistical Manual of Mental Disorders (DSM)-III-R criteria (Pritchard et al. 1991). Sampling rate of EEGs is 128 Hz. EEGs are collected under two rest states: eyes open and eyes closed. Eight-second EEG (1,024 time samples) segments free from eye blink, motion, and myogenic artifacts are extracted from the EEG recordings (one segment for each subject). The EEGs are band-limited to the range of 1–30 Hz during the EEG recording and preprocessing stages.

Results

95 PSVGs and 95 VGICs corresponding to 19 (channels) × 5 (4 EEG sub-bands and a band-limited EEG) EEGs per condition (eyes open and eyes closed) per subject (7 elderly normal and 20 AD) are obtained after the wavelet analysis and VG computations.

Statistical analysis and feature selection

The extracted PSVGs for neither eyes closed nor eyes open conditions did show significant discrimination (p value < 0.01) between the AD and normal aging groups in band-limited EEG and beta and theta EEG sub-bands. But the one-way ANOVA test showed the ability of PSVGs in alpha and delta sub-bands to distinguish AD and healthy classes. Table 1a and b presents discriminative PSVGs and the corresponding p values (p value < 0.01) in alpha and delta sub-bands, respectively. Figures 6 and 7 show the loci presented in Table 1a and b, respectively. The discriminative PSVGs in both sub-bands (alpha and delta) represent decreased FD in AD EEGs compared with elderly normal EEGs.

The extracted VGICs show significant discrimination (p value < 0.01) between the AD and normal age groups in all EEG sub-bands except one. Table 2a and b present discriminative VGICs and the corresponding p values (p value < 0.01) in eyes open (in all sub-bands) and eyes closed (in all sub-bands except beta) conditions, respectively. Table 2a shows that the discriminative VGICs in beta and theta sub-bands are increased and in alpha and delta are decreased in AD EEGs compared with elderly normal EEGs in eyes open condition. Figures 8, 9, 10, and 11

Table 1 Discriminating EEG channels obtained from PSVG (p value < 0.01)

Channel	p value	
	Eyes closed	Eyes open
(a) Alpha frequency sub-band		
Fp1	–	3.05×10^{-3}
F3	4.09×10^{-3}	–
C3	$\mathbf{1.95 \times 10^{-5}}$	–
P3	3.61×10^{-3}	–
P4	9.66×10^{-3}	–
O1	8.34×10^{-3}	–
O2	–	1.16×10^{-3}
F8	$\mathbf{1.23 \times 10^{-4}}$	9.55×10^{-3}
T3	6.04×10^{-3}	–
T6	7.99×10^{-3}	1.04×10^{-3}
Pz	–	6.27×10^{-3}
(b) Delta frequency sub-band		
C3	–	5.50×10^{-3}
O1	–	9.57×10^{-3}
F8	2.47×10^{-3}	3.05×10^{-3}
T3	–	2.21×10^{-3}
T4	$\mathbf{9.80 \times 10^{-4}}$	1.32×10^{-3}
T6	$\mathbf{2.10 \times 10^{-5}}$	2.43×10^{-3}
Fz	9.20×10^{-3}	–
Cz	$\mathbf{1.94 \times 10^{-4}}$	1.06×10^{-3}
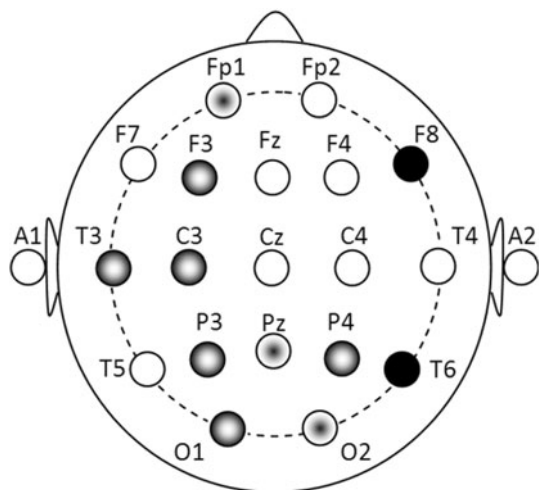
Fig. 6 Loci with discriminative PSVGs of alpha sub-band for distinguishing AD and elderly normal EEGs (p value < 0.01), in both states noted by ( ), for eyes open only ( ) and for eyes closed only ( )
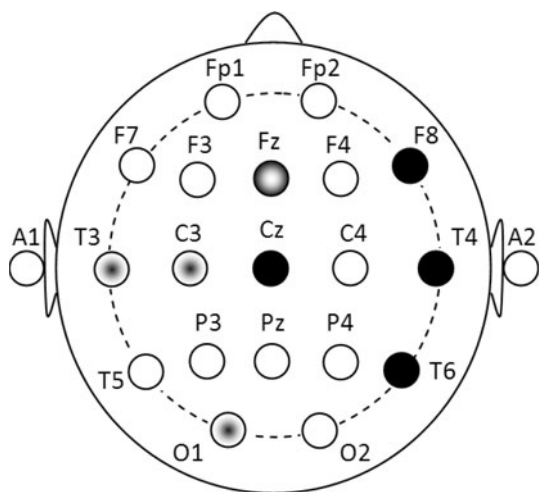
Fig. 7 Loci with discriminative PSVGs of delta sub-band for distinguishing AD and elderly normal EEGs (p value < 0.01), in both states noted by ( ), for eyes open only ( ) and for eyes close only ( )

show the loci presented in Table 2a and b for sub-bands beta, alpha, theta, and delta, respectively.

Based on ANOVA test

Using one-way ANOVA test as an open loop feature selection method, a threshold is needed for p value to find discriminative features so that the number of features is significantly less than the number of data for a meaningful classification. A smaller p value means a higher ability in

Table 2 Discriminating EEG channels obtained from VGIC (p value < 0.01)

| Channel	Sub-band	p value	Direction
(a) Eyes open			
F8	Beta	8.29×10^{-3}	Increased
F3	Alpha	6.10×10^{-3}	Decreased
P3	Alpha	9.13×10^{-3}	Decreased
T4	Alpha	6.33×10^{-3}	Decreased
Fz	Alpha	1.32×10^{-3}	Decreased
C4	Theta	1.71×10^{-3}	Increased
P3	**Theta**	$\mathbf{1.94 \times 10^{-4}}$	**Increased**
P4	Theta	6.58×10^{-3}	Increased
O1	Theta	1.37×10^{-3}	Increased
T4	Theta	1.51×10^{-3}	Increased
Fz	**Theta**	$\mathbf{7.07 \times 10^{-4}}$	**Increased**
Pz	Theta	9.14×10^{-3}	Increased
Cz	Delta	7.17×10^{-3}	Decreased
(b) Eyes closed			
F3	Alpha	8.74×10^{-3}	Decreased
P3	Alpha	7.75×10^{-3}	Decreased
F8	Alpha	5.58×10^{-3}	Decreased
P4	Theta	5.31×10^{-3}	Increased
Fz	Theta	1.56×10^{-3}	Increased
P3	Delta	1.69×10^{-3}	Increased
O2	Delta	4.01×10^{-3}	Increased
T6	**Delta**	$\mathbf{7.69 \times 10^{-4}}$	**Increased**
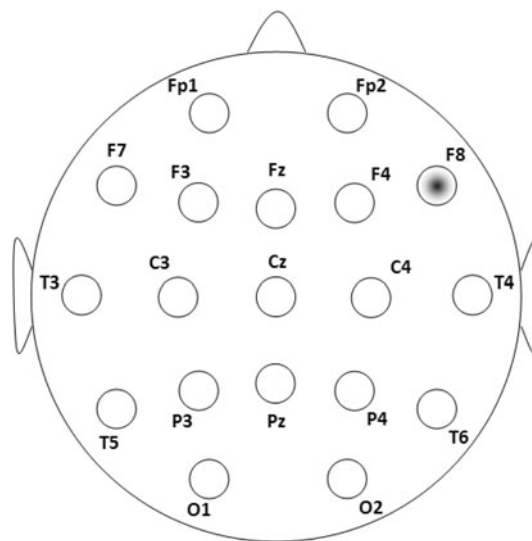
Fig. 8 Loci with discriminative VGICs of beta sub-band for distinguishing AD and elderly normal EEGs (p value < 0.01), in both states noted by ( ), for eyes open only ( ) and for eyes closed only ( )

discriminating AD and non-AD groups. Using a p value less than 10^{-3}, five PSVGs (in loci C3 and F8 in alpha band in eyes closed and T4, T6, and Cz in delta band in
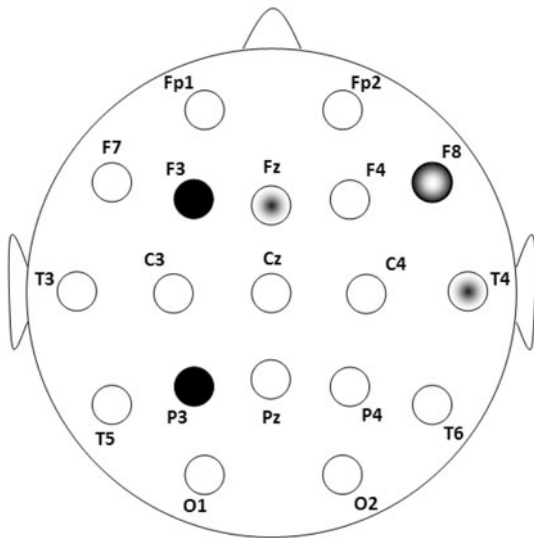
Fig. 9 Loci with discriminative VGICs of alpha sub-band for distinguishing AD and elderly normal EEGs (p value < 0.01), in both states noted by (⬤), for eyes open only (◉) and for eyes closed only (▢)
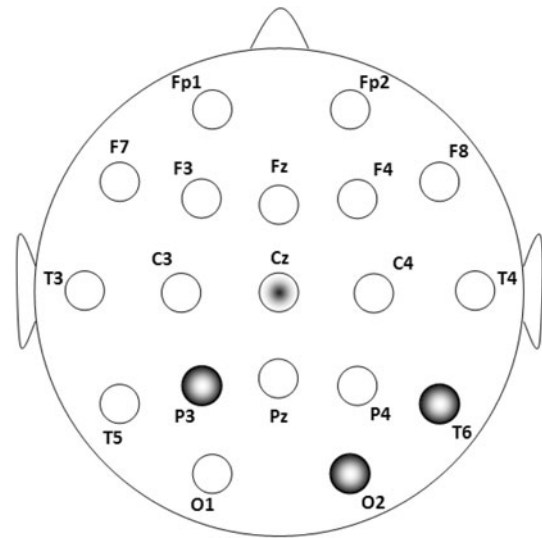
Fig. 11 Loci with discriminative VGICs of delta sub-band for distinguishing AD and elderly normal EEGs (p value < 0.01), in both states noted by (⬤), for eyes open only (◉) and for eyes closed only (▢)
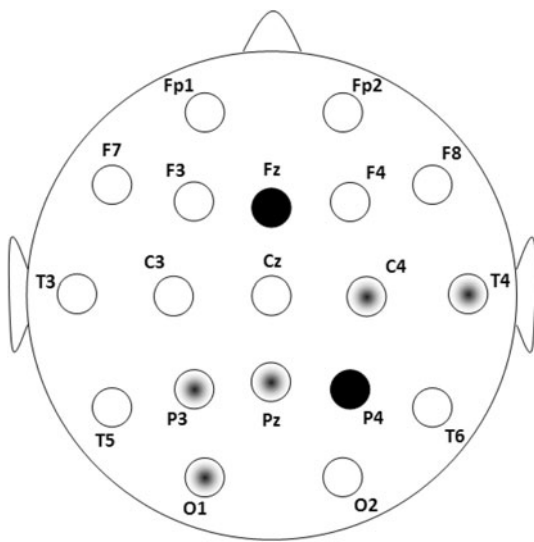
Fig. 10 Loci with discriminative VGICs of theta sub-band for distinguishing AD and elderly normal EEGs (p value < 0.01), in both states noted by (⬤), for eyes open only (◉) and for eyes closed only (▢)

eyes closed) and three VGICs (in loci P3 and Fz in theta band in eyes open and T6 in delta band in eyes closed) were found. The chosen threshold of 10^{-3} resulted in a sufficiently low number of features (8) with respect to the data number of 27 data points (7 elderly normal and 20 AD) to yield statistically meaningful classification results. These features are identified in boldface in Table 2a and b.

Classification

To evaluate the accuracy of the classification, 85% of the data (23 data) were selected randomly and used for training and the remaining 15% (4 data) were used for testing. This random selection was repeated 100 times and the average accuracy is reported. For the PCA-RBFNN classifier, using the rough guidelines mentioned earlier, three (roughly equal to 10% of the number of available data set, 27) principal components of the PCA are selected as its output for the subsequent step of RBFNN classification with three neurons in the input layer. Two other numbers were considered: four and five principal components, but no improvement in classification accuracy was achieved. Two nodes in the hidden layer of the RBFNN classifier (for both with and without PCA) were found to yield the most accurate results (a smaller number would yield less accurate results and a larger number would not improve the accuracy any further). A spread parameter (which tunes the spread of the radial basis neurons) of 3.7 was found to yield sufficient convergence in minimizing the training and testing errors for both classifiers (RBFNN and PCA-RBFNN). Table 3 presents the accuracy, sensitivity (percent of AD patients diagnosed as AD patient), and specificity (percent of healthy subjects diagnosed as healthy) for both classifications. It shows the PCA-RBFNN classifier with the input data selected by ANOVA yields the highest accuracy of $97.75 \pm 3.2\%$ with sensitivity of 100% and specificity of 91.08% for diagnosis of the AD. This accuracy is considerably higher than the accuracy of

Table 3 Results of classifications

Classifier	Accuracy (%)	Standard deviation (%)	Sensitivity (%)	Specificity (%)
RBFNN	96.50	4.1	100	87.03
PCA-RBFNN	97.75	3.2	100	91.08

87.8% reported recently by Gomez et al. (2009) based on MEG records and FD.

Conclusion

Complexity in EEG and MEG records is an effective criterion to reveal changes in the dynamics of AD brain caused by loss of neuronal synapses and cortical changes (Geula and Mesulam 1996; Lerch et al. 2005; Fjell et al. 2009; Kuczynski et al. 2010; Stephen et al. 2010). Decreased complexity of the AD EEGs in various regions of the brain in the band-limited EEGs has been reported by a number of researchers based on CD and FD but not with high accuracy. Two reasons can be cited for this: (1) lack of an effective measurement tool for complexity of EEG and MEG, and (2) lack of comprehensive assessment of the measurements. For example, up to now, no results were reported on the investigation of FD in EEG and MEG sub-bands.

Recently, VG algorithm has been introduced as a simple but powerful algorithm to convert time series to graphs while preserving the dynamic characteristics such as complexity. The research presented in this paper confirmed the authors' hypothesis that complexity of VGs in certain EEG sub-bands presents significant differences between AD patient and control individuals.

A new chaos–wavelet approach is presented for EEG-based diagnosis of AD employing VG. After comprehensive statistical studies, effective classification features and mathematical markers were discovered. Finally, using a two-stage classifier (PC-RBFNN), a high accuracy of 97.7% was obtained using the selected features obtained via ANOVA. Interestingly, the nonlinear features selected by ANOVA are from delta, theta, and alpha sub-bands whose powers recently were reported as promising EEG markers of disease progression in Mild Cognitive Impairment (MCI) and mild AD (Jackson and Snyder 2008). Increased fractality in theta and delta and decreased fractality in alpha show correlation with conventional linear characteristics, called EEG slowing, in AD as well. The brain damage was found mostly in the temporal lobes (T4 and T6), some loci in the central regions (C3 and Cz), some in the loci in frontal lobe (F8 and Fz), and P3 in the left parietal lobe. The temporal lobes have the most critical role in episodic memory which is seriously affected in AD.

Recently, an MRI-based study suggested medial temporal lobe atrophy as a suitable characteristic for distinguishing the Alzheimer's disease from other dementias (dementia with Lewy bodies and vascular dementia) (Burton et al. 2009). The deficit in the dynamics of the temporal lobes discovered in this research implies deficits of AD in episodic memory. The deficiencies found in the central regions may be related to sensory-motor coordination in AD. Deficits in dynamic of frontal lobes generally may lead to deficits in different high level processing such as planning and managing emotions. Damage to the left parietal lobe may impair integration and processing of the sensory information associated with language production and object perception.

The local and global structural changes and impairments in a complex system such as brain affect its dynamical characteristics especially its complexity. Recent MRI-based findings report differences of structural impairments and atrophy patterns in different dementias (Barber et al. 2001; Meyer et al. 2007; Whitwell et al. 2007; Burton et al. 2009). The research presented in this paper offers a comprehensive method for detecting impaired loci and frequency bands in the context of complexity that can be used as an alternative to distinguish AD from the other dementias based on EEG. Also, in addition to diagnostic value, the discovered biomarkers would be more accurate in monitoring and evaluating long-term treatment methods of AD than quantitative EEG markers such as the mean absolute theta and beta 1 (12–15.5 Hz) powers (Kogan et al. 2001).

The authors have, in fact, presented a general methodology for EEG-based diagnosis of the neurological orders that can be used for automated diagnosis of other neurological and psychiatric disorders such as attention deficit hyperactivity disorder (ADHD) (Ahmadlou and Adeli 2010) and autism spectrum disorder (ASD).

References

Adeli H, Zhou Z, Dadmehr N (2003) Analysis of EEG records in an epileptic patient using wavelet transform. J Neurosci Methods 123(1):69–87

Adeli H, Ghosh-Dastidar S, Dadmehr N (2005a) Alzheimer's disease: models of computation and analysis of EEGs. Clin EEG Neurosci 36(3):131–140

Adeli H, Ghosh-Dastidar S, Dadmehr N (2005b) Alzheimer's disease and models of computation: imaging, classification, and neural models. J Alzheimer's Dis 7(3):187–199

Adeli H, Ghosh-Dastidar S, Dadmehr N (2007) A wavelet–chaos methodology for analysis of EEGs and EEG subbands to detect seizure and epilepsy. IEEE Trans Biomed Eng 54(2):205–211

Adeli H, Ghosh-Dastidar S, Dadmehr N (2008) A spatio-temporal wavelet–chaos methodology for EEG-based diagnosis of Alzheimer's disease. Neurosci Lett 444(2):190–194

Adler G, Brassen S, Jajcevic A (2003) EEG coherence in Alzheimer's dementia. J Neural Transm 110(9):1051–1058

Ahmadlou M, Adeli H (2010) Wavelet-synchronization methodology: a new approach for EEG-based diagnosis of ADHD. Clin EEG Neurosci 41(1):1–10

Anand P, Siva Prasad BVN, Venkateswarlu C (2009) Modeling and optimization of a pharmaceutical formulation system using radial basis function network. Int J Neural Syst 19(2):127–136

Barber R, McKeith IG, Ballard C, Gholkar A, O'Brien JT (2001) A comparison of medial and lateral temporal lobe atrophy in dementia with Lewy bodies and Alzheimer's disease: magnetic resonance imaging volumetric study. Dement Geriatr Cogn Disord 12(3):198–205

Besthorn C, Sattel H, Geiger-Kabisch C, Zerfass R, Förstl H (1995) Parameters of EEG dimensional complexity in Alzheimer's disease. Electroencephalogr Clin Neurophysiol 95(2):84–89

Besthorn C, Zerfass R, Geiger-Kabisch C, Sattel H, Daniel S, Schreiter-Gasser U, Forstl H (1997) Discrimination of Alzheimer's disease and normal aging by EEG data. Electroencephalogr Clin Neurophysiol 103(2):241–248

Bouwman FH, Schoonenboom NSM, Verwey NA, Elk EJ, Kok A, Blankenstein MA, Scheltens P, Flier WM (2009) CSF biomarker levels in early and late onset Alzheimer's disease. Neurobiol Aging 30(12):1895–1901

Burton EJ, Barber R, Mukaetova-Ladinska EB, Robson J, Perry RH, Jaros E, Kalaria RN, O'Brien JT (2009) Medial temporal lobe atrophy on MRI differentiates Alzheimer's disease from dementia with Lewy bodies and vascular cognitive impairment: a prospective study with pathological verification of diagnosis. Brain 132(1):195–203

Deursen JA, Vuurman EFPM, Verhey FRJ, Kranen-Mastenbroek VHJM, Riedel WJ (2008) Increased EEG gamma band activity in Alzheimer's disease and mild cognitive impairment. J Neural Transm 115(9):1301–1311

Deursen JA, Vuurman EFPM, Kranen-Mastenbroek VHJM, Verhey FRJ, Riedel WJ (2009) 40-Hz steady state response in Alzheimer's disease and mild cognitive impairment. Neurobiol Aging. doi:10.1016/j.neurobiolaging.2009.01.002

Dierks T, Jelic V, Julin P, Maurer K, Wahlund LO, Almkvist O, Strik WK, Winblad B (1997) EEG-microstates in mild memory impairment and Alzheimer's disease: possible association with disturbed information processing. J Neural Transm 104(4–5):483–495

Fjell AM, Westlye LT, Amlien I, Espeseth T, Reinvang I, Raz N, Agartz I, Salat DH, Greve DN, Fischl B, Dale AM, Walhovd KB (2009) High consistency of regional cortical thinning in aging across multiple samples. Cereb Cortex 19(9):2001–2012

Fjell AM, Walhovd KB, Fennema-Notestine C, McEvoy LK, Hagler DJ, Holland D, Blennow K, Brewer JB, Dale AM (2010) Brain atrophy in healthy aging is related to CSF levels of Aβ1-42. Cerebral Cortex. doi:10.1093/cercor/bhp279

Geula C, Mesulam MM (1996) Systematic regional variations in the loss of cortical cholinergic fibers in Alzheimer's disease. Cereb Cortex 6(2):165–177

Ghosh-Dastidar S, Adeli H, Dadmehr N (2008) Principal component analysis-enhanced cosine radial basis function neural network for robust epilepsy and seizure detection. IEEE Trans Biomed Eng 55(2):512–518

Giannitrapani D, Collins J, Vassiliadis D (1991) The EEG spectra of Alzheimer's disease. Int J Psychophysiol 10(3):259–269

Gomez C, Mediavilla A, Hornero R, Abasolo D, Fernandez A (2009) Use of the Higuchi's fractal dimension for the analysis of MEG recordings from Alzheimer's disease patients. Med Eng Phys 31(3):306–313

Hampel H, Teipel SJ, Alexander GE, Pogarell O, Rapoport SI, Möller HJ (2002) In vivo imaging of region and cell type specific neocortical neurodegeneration in Alzheimer's disease. J Neural Transm 109(5–6):837–855

He Z, You X, Zhou L, Cheung Y, Tang YY (2010) Writer identification using fractal dimension of wavelet subbands in Gabor domain. Integr Comput Aided Eng 17(2):157–165

Head D, Snyder AZ, Girton LE, Morris JC, Buckner RL (2005) Frontal-hippocampal double dissociation between normal aging and Alzheimer's disease. Cereb Cortex 15(6):732–739

Hiele K, Vein AA, Welle A, Grond J, Westendorp RGJ, Bollen ELEM, Buchem MA, Dijk JG, Middelkoop HAM (2007) EEG and MRI correlates of mild cognitive impairment and Alzheimer's disease. Neurobiol Aging 28(9):1322–1329

Higuchi T (1988) Approach to an irregular time series on the basis of the fractal theory. Physica D Nonlinear Phenom 31(2):277–283

Jackson CE, Snyder PJ (2008) Electroencephalography and event-related potentials as biomarkers of mild cognitive impairment and mild Alzheimer's disease. Alzheimer's Dementia 4(1–1):137–143

Jelles B, van Birgelen JH, Slaets JPJ, Hekster REM, Jonkman EJ, Stam CJ (1999) Decrease of non-linear structure in the EEG of Alzheimer patients compared to healthy controls. Clin Neurophysiol 110(7):1159–1167

Jeong J, Chae JH, Kim SY, Han SH (2001) Nonlinear dynamic analysis of the EEG in patients with Alzheimer's disease and vascular dementia. J Clin Neurophysiol 18(1):58–67

Jones BF, Barnes J, Uylings HB, Fox NC, Frost C, Witter MP, Scheltens P (2006) Differential regional atrophy of the cingulate gyrus in Alzheimer disease: a volumetric MRI study. Cereb Cortex 16(12):1701–1708

Junfei Q, Honggui H (2010) A repair algorithm for radial basis function neural network with application to chemical oxygen demand modeling. Int J Neural Syst 20(1):63–74

Karim A, Adeli H (2003) Radial basis function neural network for work zone capacity and queue estimation. J Transp Eng 129(5):494–503

Kim J, Wilhelm T (2008) What is a complex graph? Physica A Stat Mech Appl 387(11):2637–2652

Kogan EA, Korczyn AD, Virchovsky RG, Klimovizky SS, Treves TA, Neufeld MY (2001) EEG changes during long-term treatment with donepezil in Alzheimer's disease patients. J Neural Transm 108(10):1167–1173

Kramer MA, Chang FL, Cohen ME, Hudson D, Szeri AJ (2007) Synchronization measures of the scalp EEG can discriminate healthy from Alzheimer's subjects. Int J Neural Syst 17(2):61–69

Kuczynski B, Targan E, Madison C, Weiner M, Zhang Y, Reed B, Chui HC, Jagust W (2010) White matter integrity and cortical metabolic associations in aging and dementia. Alzheimer's Dementia 6(1):54–62

Lacasa L, Luque B, Ballesteros F, Luque J, Nuno JC (2008) From time series to complex networks: the visibility graph. Proc Natl Acad Sci USA 105(13):4972–4975

Lacasa L, Luque B, Luque J, Nuno JC (2009) The visibility graph: a new method for estimating the Hurst exponent of fractional Brownian motion. Europhys Lett 86(3):30001–30004

Lee H, Cichocki A, Choi S (2007) Nonnegative tensor factorization for continuous EEG classification. Int J Neural Syst 17(4):305–317

Lerch JP, Pruessner JC, Zijdenbos A, Hampel H, Teipel SJ, Evans AC (2005) Focal decline of cortical thickness in Alzheimer's disease identified by computational neuroanatomy. Cereb Cortex 15(7):995–1001

Lipovetsky S (2009) PCA and SVD with nonnegative loadings. Pattern Recogn 42(1):68–76

Lopez-Rubio E, Ortiz-de-Lazcano-Lobato JM (2009) Dynamic competitive probabilistic principal components analysis. Int J Neural Syst 19(2):91–103

Meyer JS, Huang J, Chowdhury MH (2007) MRI confirms mild cognitive impairments prodromal for Alzheimer's, vascular and Parkinson–Lewy body dementias. J Neurol Sci 257(1–2):97–104

Osipova D, Pekkonen E, Ahveninen J (2006) Enhanced magnetic auditory steady-state response in early Alzheimer's disease. Clin Neurophysiol 117(9):1990–1995

Osterhage H, Mormann F, Wagner T, Lehnertz K (2007) Measuring the directionality of coupling: phase versus state space dynamics and application to EEG time series. Int J Neural Syst 17(3):139–148

Pedrycz W, Rai R, Zurada J (2008) Experience-consistent modeling for radial basis function neural networks. Int J Neural Syst 18(4):279–292

Pritchard WS, Duke DW, Coburn KL (1991) Altered EEG dynamical responsivity associated with normal aging and probable Alzheimer's disease. Dementia 2(2):102–105

Rossello JL, Canals V, Morro A, Verd J (2009) Chaos-based mixed signal implementation of spiking neurons. Int J Neural Syst 19(6):465–471

Savitha R, Suresh S, Sundararajan N (2009) A fully complex-valued radial basis function network and its learning algorithm. Int J Neural Syst 19(4):253–267

Stebbins GT, Murphy CM (2009) Diffusion tensor imaging in Alzheimer's disease and mild cognitive impairment. Behav Neurol 21(1):39–49

Stephen JM, Montano R, Donahue CH, Adair JC, Knoefel J, Qualls C, Hart B, Ranken D, Aine CJ (2010) Somatosensory responses in normal aging, mild cognitive impairment, and Alzheimer's disease. J Neural Transm 117(2):217–225

Thomas C, Berg I, Rupp A, Seidl U, Schroder J, Roesch-Ely D, Kreisel SH, Mundt C, Weisbrod M (2010) P50 gating deficit in Alzheimer dementia correlates to frontal neuropsychological function. Neurobiol Aging 31(3):416–424

Thompson PM, Moussai J, Zohoori S, Goldkorn A, Khan AA, Mega MS, Small GW, Cummings JL, Toga AW (1998) Cortical variability and asymmetry in normal aging and Alzheimer's disease. Cereb Cortex 8(6):492–509

Thompson PM, Mega MS, Woods RP, Zoumalan CI, Lindshield CJ, Blanton RE, Moussai J, Holmes CJ, Cummings JL, Toga AW (2001) Cortical change in Alzheimer's disease detected with a disease-specific population-based brain atlas. Cereb Cortex 11(1):1–16

Whitwell JL, Weigand SD, Shiung MM, Boeve BF, Ferman TJ, Smith GE, Knopman DS, Petersen RC, Benarroch EE, Josephs KA, Jack CR Jr (2007) Focal atrophy in dementia with Lewy bodies on MRI: a distinct pattern from Alzheimer's disease. Brain 130(3):708–719

Woyshville MJ, Calabrese JR (1994) Quantification of occipital EEG changes in Alzheimer's disease utilizing a new metric: the fractal dimension. Biol Psychiatry 35(6):381–387

Wu Q, Ben-Arie J (2008) View invariant head recognition by hybrid PCA based reconstruction. Integr Comput Aided Eng 15(2)97–108

Wu D, Warwick K, Ma Z, Gasson MN, Burgess JG, Pan S, Aziz TZ (2010) Prediction of Parkinson's disease tremor onset using radial basis function neural network based on particle swarm optimization. Int J Neural Syst 20(2):109–116